WILEY-VCH

Electrosprayed regeneration-enhancer-element microspheres power osteogenesis and angiogenesis coupling

*Tianpeng Xu, Yuhe Yang, Di Suo, Ho Pan Bei, Xiaoxiao Xu, Xin Zhao**

T. Xu., Dr. Y. Yang., D. Suo., H. P. Bei., X. Xu., Dr. X. Zhao.
Department of Biomedical Engineering, The Hong Kong Polytechnic University, Hung Hom, Hong Kong SAR, China
Email: xin.zhao@polyu.edu.hk

Key words: electrosprayed microspheres, regeneration-enhancer-element, osteogenesis, angiogenesis, bone regeneration

Abstract: Electrosprayed microspheres for bone regeneration are conventionally restricted by the lack of osteogenic modulation for both encapsulated stem cells and surrounding cells at the defect site. Here, we electrospray sodium alginate microspheres encapsulating L-arginine doped hydroxyapatite nanoparticles (Arg/HA NPs) and rat bone mesenchymal stem cells (rBMSCs) as regeneration-enhancer-element reservoirs (Arg/HA-SA@BMSC) for bone healing. The Arg/HA NPs serve as a container of L-arginine and Ca^{2+} and the rBMSCs inside the microspheres could metabolize the released L-arginine into bioactive gas nitric oxide (NO) in the presence of Ca^{2+} to activate the nitric oxide (NO)/cyclic guanosine monophosphate (cGMP) signaling pathway. Meanwhile, the generated NO could diffuse out of the microspheres together with the Ca^{2+} and L-arginine as exterior enhancers to promote the osteogenesis-angiogenesis coupling of surrounding rBMSCs and endothelial cells (ECs) at the bone defect site, generating an internal/external modulation loop between the encapsulated cells and surrounding native cells. We demonstrate such regeneration-enhancer-element reservoirs could effectively increase the bone tissue formation and neovasculature using rat calvarial defect models. We envision that our microsphere system could streamline the vascularized bone regeneration therapy as a high throughput, minimal invasive yet highly effective strategy to accelerate bone healing.

1. Introduction

Stem cell injection has emerged as a promising treatment strategy in bone regeneration due to its minimal invasiveness (injectability) and encouraging therapeutic performance in accelerating bone reconstruction.[1] However, the efficacy of direct injection of stem cells can be compromised due to the damage from shear stress and the uncontrolled dispersion of stem cells.[2] Encapsulation of stem cells inside microspheres has thus been adopted for increased cell viability and limited cell dispersion.[3] Current cell-laden microspheres are mostly fabricated by emulsion and microfluidics techniques.[4] Although emulsion allows for scalable production, the high shear stress could hamper cell viability and it is difficult to generate microspheres with narrow size distribution.[5] Microfluidics approach can produce uniform microspheres; however, its clinical application is drastically impeded by the low productivity and high cost.[6] Alternatively, electrospraying has since attracted significant attention as an alternative solution due to its high production speed and massive yield with controllable size distribution.[7] Recently, various hydrogel materials including poly(ethylene glycol) diacrylate (PEGDA),[8] gelatin methacryloyl[6] or sodium alginate[9] have been reported to successfully encapsulate cells with high viability by electrospraying.[10] Unfortunately, most of the present electrosprayed microspheres lack appropriate stimulation to guide the regenerative fate of the encapsulated cells. More importantly, these studies only considered the modulation of encapsulated cells but overlooked the potential role of microspheres as a modulator for surrounding cells in the defect site through cell-cell/cell-material communication.[11] To this end, the microspheres could possibly serve as reservoirs to establish a native homeostasis feedback cycle between the encapsulated cells and the surrounding cells; however, fabrication of such self-sufficient, cell-powered microspheres to initiate inter-linked modulation loop between the inside and outside for bone regeneration has never been reported.

In this regard, we propose to electrospray microspheres encapsulating stem cells and natural tissue metabolites as integrated regeneration-enhancer-element reservoirs to power the

inside/outside cell-cell/cell-material communication loop for accelerated bone tissue repair. As a proof of concept, we prepare sodium alginate (SA) microspheres encapsulating bone mesenchymal stem cells (BMSCs) and L-arginine doped hydroxyapatite nanoparticles (Arg/HA NPs) as integrated regeneration-enhancer-element reservoirs (Arg/HA-SA@BMSC) to power the osteogenesis-angiogenesis coupling at the defect site during bone regeneration (**Figure 1**). The SA hydrogel is FDA approved with excellent biocompatibility.[12] The Arg/HA NPs supply the natural metabolizable enhancer element, L-arginine and calcium ion (Ca^{2+}), which has proven capability to activate the nitric oxide (NO)/cyclic guanosine monophosphate (cGMP) signaling pathway in both BMSCs and endothelial cells (ECs) for a well-coordinated osteogenesis-angiogenesis coupling during bone reconstruction.[13] In our proposed system, the BMSCs inside the microspheres could metabolize the released L-arginine into NO as a modulation messenger in the presence of Ca^{2+}.[13-14] Then, the metabolized NO could serve as an interior enhancer to promote the osteogenesis of encapsulated BMSCs by activating the NO/cGMP signaling pathway.[14] The resultant NO also diffuses out of the microspheres together with the Ca^{2+} and L-arginine to work as an exterior enhancer to power the osteogenesis-angiogenesis coupling of surrounding BMSCs and ECs in the bone regeneration. To the best of our knowledge, this is the first study to develop cell-laden microspheres with only endogenous elements of the human body to initiate inter-linked modulation loop between the inside and outside, i.e., to modulate the behaviors of cells inside and outside the microspheres for bone regeneration. Our cell-laden and Arg/HA NP loaded microspheres could not only enhance the osteogenesis of encapsulated BMSCs but also realize the exterior cells' osteogenic and angiogenic potential. We demonstrate our Arg/HA-SA@BMSC microspheres' capability to accelerate new bone formation and neovascularization in a rat calvarial defect model. We envision that our microsphere system could streamline the vascularized bone regeneration therapy as a high throughput, minimal invasive yet highly effective stragety to accelerate vascularized bone healing.

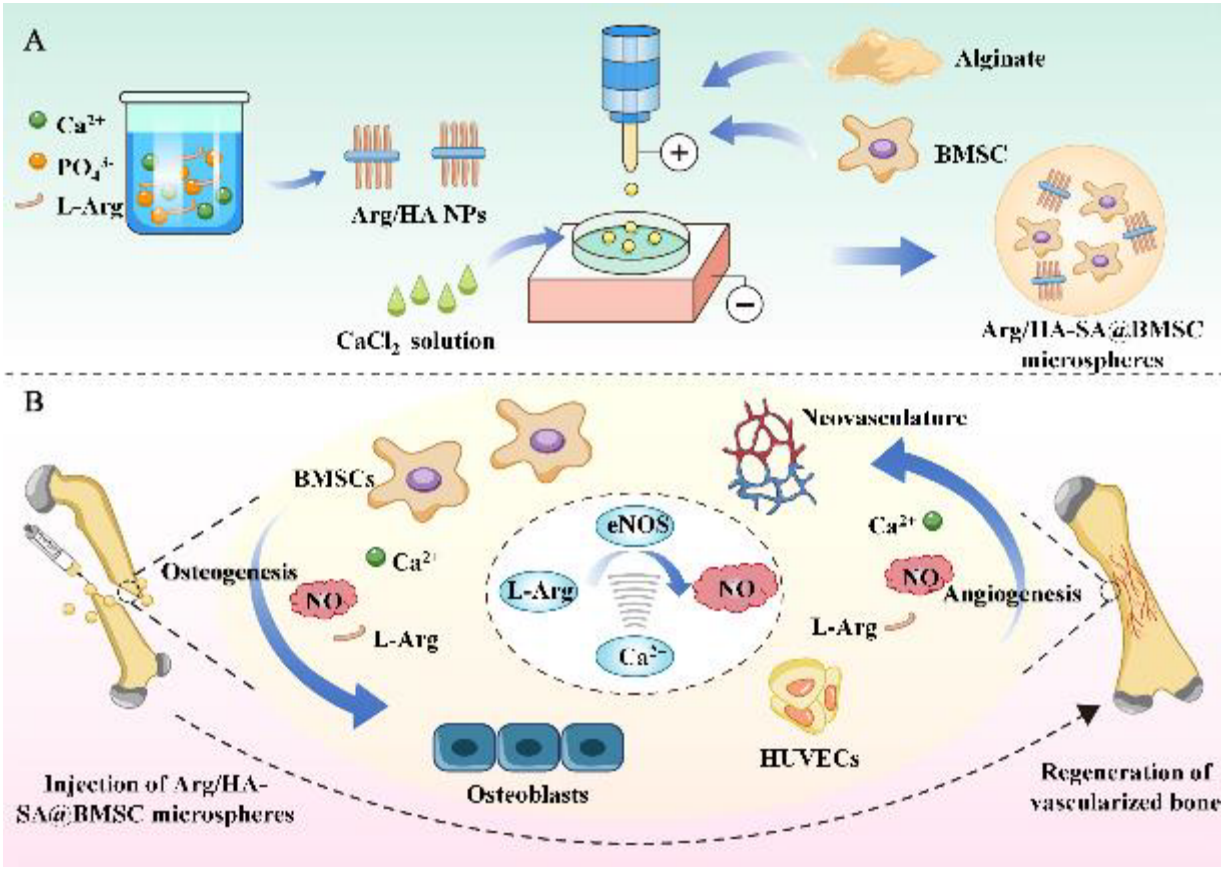

Figure 1. Schematic illustration of the electrosprayed regeneration-enhancer-element reservoirs to power the osteogenesis-angiogenesis coupling in bone regeneration. (A) The regeneration-enhancer-element reservoirs are fabricated by electrospraying composite hydrogels composed of sodium alginate (SA), bone mesenchymal stem cells (BMSCs) and L-arginine doped hydroxyapatite nanoparticles (Arg/HA-SA). (B) The regeneration-enhancer-element reservoirs can not only promote the osteogenesis of encapsulated BMSCs by metabolizing the released L-arginine into bioactive gas nitric oxide (NO) and activating the NO/cGMP signaling pathway, but also enhance the osteogenesis-angiogenesis coupling of surrounding BMSCs and ECs through the release of NO, Ca^{2+} and L-arginine from the microspheres.

2. Results and discussion

We firstly synthesized L-arginine doped hydroxyapatite nanoparticles (Arg/HA NPs) as the source of L-arginine and calcium ion (Ca^{2+}) with varied L-arginine doping concentration from

0.01 M to 0.25 M. To evaluate the morphology of the synthesized Arg/HA NPs, we performed transmission electron microscope (TEM) analysis and found that the HA NPs with no L-arginine, 0.01M Arg/HA, and 0.05 M Arg/HA groups presented rod-like shape with good dispersion; however, severe aggregation was observed when the doping concentration of L-arginine reached 0.1 M, which could block the needle in the electrospray process (**Figure 2A**). Such aggregation tendency could be attributed to the significantly decreased average diameter from 149.34 ± 23.21 (HA NPs), 132.16 ± 31.33 nm (0.01M Arg/HA NPs), 118.44 ±28.16 nm (0.05M Arg/HA NPs) to 67.13 ± 8.16 nm (0.1M Arg/HA NPs) as presented by dynamic light scattering (DLS) analysis (**Figure 2D**). To illustrate the successful binding between HA and L-arginine, we adopted Fourier transform infrared spectroscopy (FTIR) evaluation and found the characteristic peaks at 1455 cm^{-1} and 2900-2800 cm^{-1} denoting "N-H" and "C-H" bonds in L-arginine appearing in all Arg/HA groups,[15] indicating that L-arginine has been successfully immobilized onto HA NPs (**Figure 2B**). We further performed X-ray diffraction (XRD) spectrometry and found that all groups showed the structural phase of pure HA with characteristic peaks at (0 0 2), (2 1 1), (3 0 0), (2 0 2), (3 1 0), (2 2 2), and (2 1 3) without any shifts or new peaks,[16] showing the successful formation of crystalline HA after the L-arginine doping (**Figure 2C**).

We then moved on to the analysis of release kinetics of L-arginine and Ca^{2+} from the synthesized Arg/HA NPs and found that both molecules were long-term released over 28 days. Compared with pure HA, L-arginine doped groups presented relatively faster Ca^{2+} release possibly because the hydrophilic L-arginine could accelerate the HA disintegration (**Figure 2E and F**).[17] As expected, the amount of released L-arginine over time increased with L-arginine doping concentration. Altogether, we demonstrated the successful synthesis of Arg/HA NPs. In consideration of the Arg/HA NP morphology and release kinetics, we selected the 0.05 M Arg/HA NPs (denoted as Arg/HA below) for the following fabrication of electrosprayed microspheres.

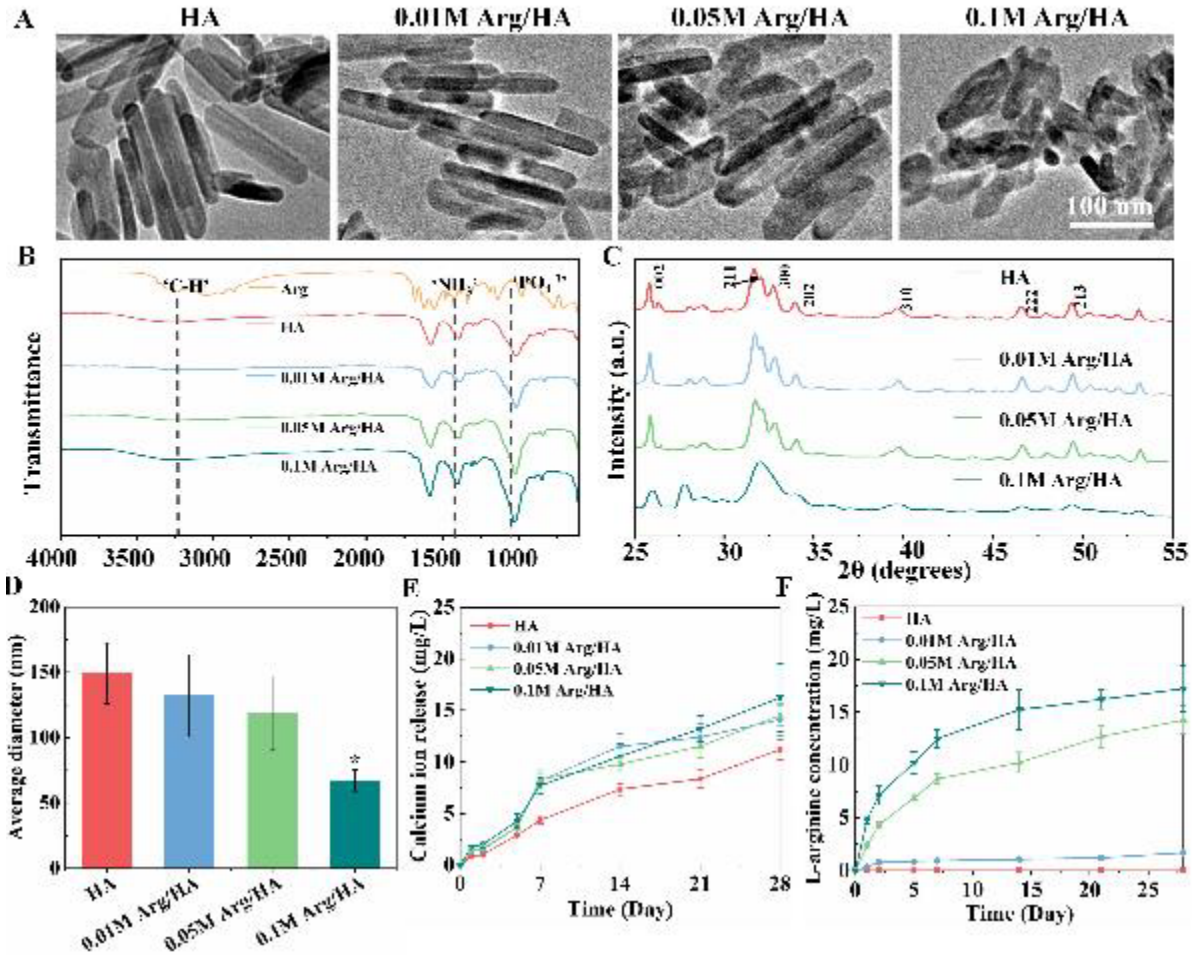

Figure 2. Characterization of the synthesized Arg/HA NPs. (A) Representative TEM images of Arg/HA NPs with different L-arginine doping concentration. (B) FTIR spectra of L-arginine, HA and Arg/HA NPs with different L-arginine doping concentration. (C) XRD spectra and (D) average diameter of HA and different Arg/HA NPs. (E) Ca^{2+} and (F) L-arginine release from the HA and Arg/HA NPs for 28 days. Sample size $n = 3$ for all experiments. Data are analyzed by a one-way ANOVA with a Tukey's post hoc test for multiple comparison. Data are presented as mean ± SD. *$p < 0.05$ is considered significantly different compared with the HA group.

We then electrosprayed Arg/HA-SA microspheres with varying Arg/HA loading and used naked SA microspheres as control. After optimization of electrospraying parameters, we obtained pure SA microspheres with diameter ranging from 150 μm to 250 μm (**Figure 3A and B**). After incorporating 0.5% and 1% Arg/HA, the microspheres still presented suitable

diameter distribution (209 ± 21.73 μm and 219 ± 21.05 μm); however, the 2% Arg/HA-SA group showed drastically decreased microsphere diameter with nonuniform size distribution (122.9 ± 31.16 μm). This may be attributed to the overloaded Arg/HA, compromising the stability of the electrospraying process and obstructing the syringe needle. To ensure the Arg/HA-SA microspheres are mechanically stable and could bear the inevitable shear force during the injection process, we performed the microcompression tests to evalute the Young's modulus of different micropheres and found that the modulus of the SA micropheres was 3.73 ± 0.36 kPa. After incorporation of Arg/HA, we observed a significant increase of modulus to 5.32 ± 0.66, 7.12 ± 0.87 and 8.36 ± 1.03 kPa for 0.5% Arg/HA-SA, 1% Arg/HA-SA and 2% Arg/HA-SA micropheres respectively (**Figure S1**)**.** All groups presented satisfactory mechanical properties to maintain the shape of microspheres during injection. We further investigated the degradation of the microspheres. As shown in **Figure S2**, the microspheres of pure SA group were intact for more than 21 days after immersion in PBS. After the addition of Arg/HA, the degradation was accelerated due to the enhanced swelling of the microspheres. For 1% Arg/HA-SA group, the microspheres showed small fragmentations on day 14 and were completely broken on day 21. When the concentration of Arg/HA reached 2%, the microspheres degraded completely by day 14. Altogether, the 1% Arg/HA-SA microspheres presented the suitable size distribution and satisfactory mechanical properties for cell encapsulation and were therefore adopted for the following studies.

Next, we encapsulated rBMSCs in the Arg/HA-SA microspheres to prepare the integrated regeneration-enhancer-element reservoirs. We firstly evaluated the biocompatibility of the Arg/HA-SA microspheres in terms of cell viability and proliferation. The viability of encapsulated rBMSCs in all groups maintained over 90% during the 7-day incubation period, indicating excellent cytocompatibility of the materials (**Figure 3C and D**). We also evaluated the cell proliferation via PicoGreen assay and found that all the microspheres could support cell proliferation. The 1% Arg/HA-SA group presented significantly higher cell proliferation

compared to the SA group on day 7 (**Figure 3E**). This may be attributed to the synthesis of bioactive gas NO with the supplement of L-arginine that could promote cell proliferation. We then performed F-actin staining to observe the cell morphology and migration status in the microspheres. We found that all cells presented round morphology without obvious sprouting and elongating due to the lack of adhesion sites of alginate for cell binding.[18] In terms of cell migration, we found more cells migrated to the edge of the microspheres in the Arg/HA-SA groups compared with the SA group (**Figure 3F and G**). To investigate the cell release capacity of the microspheres, we continuously incubated the microspheres with rBMSC encapsulation for 28 days (**Figure S3**). We found that the released cell density of Arg/HA-SA microspheres was 4.12 fold and 1.5 fold higher compared to the SA and HA-SA microspheres after 28 days, demonstrating that the Arg/HA-SA microspheres could provide preferable microenvironment for the cell growth and migration (**Figure 3H**).

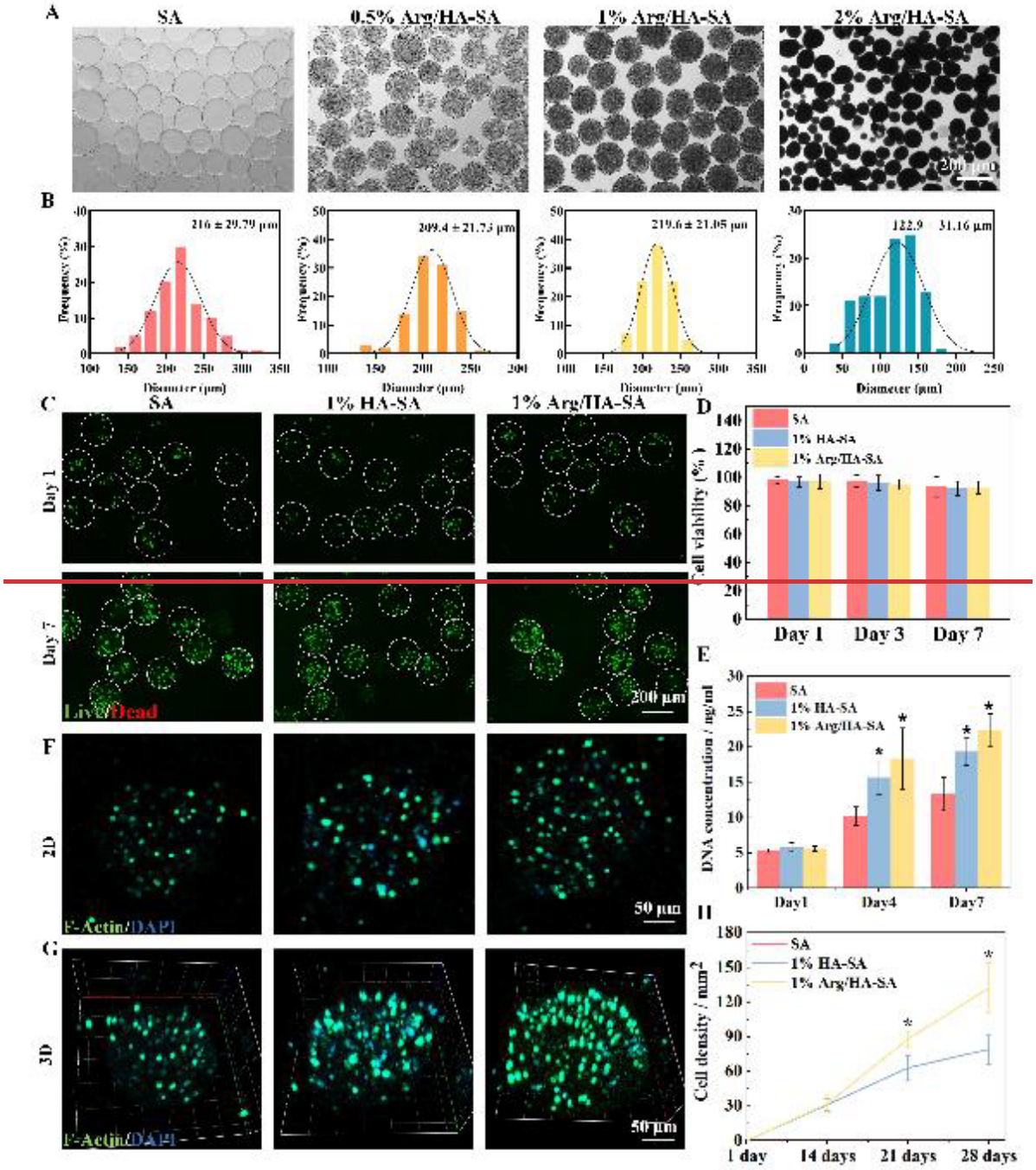
A
SA
0.5% Arg/HA-SA
1% Arg/HA-SA
2% Arg/HA-SA
200 μm
B
216 ± 29.79 μm
209.4 ± 21.73 μm
219.6 ± 21.05 μm
122.9
31.16 μm
Frequency (%)
Diameter (μm)
C
SA
1% HA-SA
1% Arg/HA-SA
Day 1
Day 7
Live/Dead
200 μm
D
SA
1% HA-SA
1% Arg/HA-SA
Cell viability (%)
Day 1
Day 3
Day 7
E
SA
1% HA-SA
1% Arg/HA-SA
DNA concentration / ng/ml
Day1
Day4
Day7
F
2D
F-Actin/DAPI
50 μm
G
3D
F-Actin/DAPI
50 μm
H
SA
1% HA-SA
1% Arg/HA-SA
Cell density / mm^2
1 day
14 days
21 days
28 days

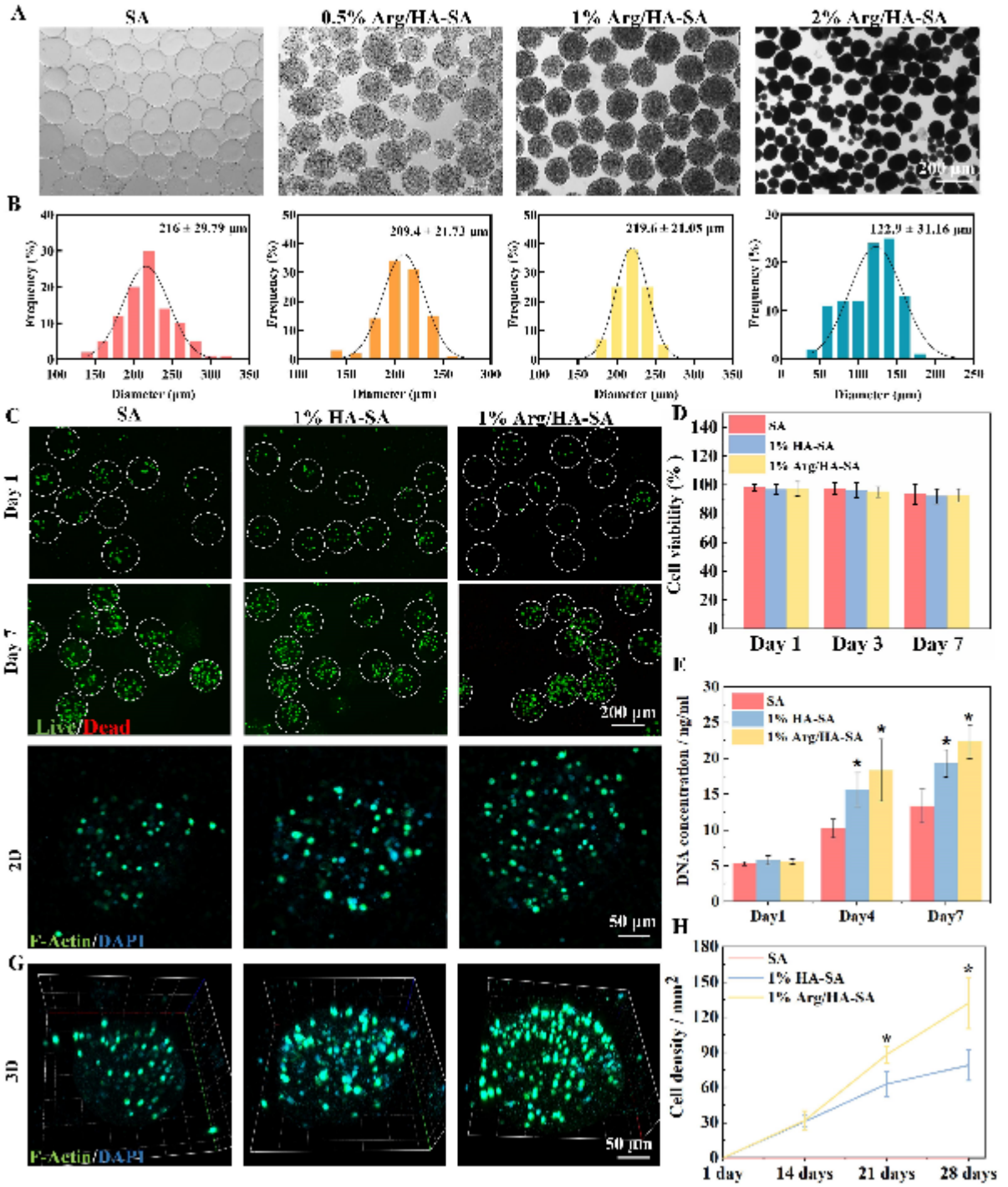

Figure 3. Characterization of fabricated Arg/HA-SA microspheres. (A) Morphology and (B) size distribution of Arg/HA-SA microspheres with different Arg/HA loading concentration. (C) Live/Dead staining of rBMSCs encapsulated in different microspheres on day 1 and 7. Green and red fluorescence denote live and dead cells, respectively and white circle denotes the microspheres. Quantitative evaluation of (D) cell viability and (E) DNA concentration of different microspheres on day 1, 3 and 7. (F) 2D and (G) 3D phalloidin staining images of

rBMSCs encapsulated in different microspheres on day 7. (H) Quantification of the cell release density of rBMSCs in different microspheres. Sample size $n = 3$ for all experiments. Data are analyzed by a two-way ANOVA with a Tukey's post hoc test for multiple comparison. Data are presented as mean ± SD. *$p < 0.05$ is considered significantly different compared with the SA group.

On account of the excellent biocompatibility of the microspheres, we next assessed the enhancement effect of Arg/HA on osteogenesis of rBMSCs inside the regeneration-enhancer-element reservoirs. We performed the alkaline phosphatase (ALP) analysis as an early osteogenesis metabolism marker. Compared with pure SA, the HA-SA group exhibited more ALP positive staining area on day 3 and 7 (**Figure 4A**). In addition, the Arg/HA-SA groups showed further increase of ALP staining area on both time points. Quantitively, the ALP activity of the Arg/HA-SA group was 3.06 and 1.52 folds higher compared with the SA and HA-SA group on day 7, displaying the best early osteogenesis potential (**Figure 4C**). The calcium mineral deposition was further evaluated by alizarin red S (ARS) staining in which the Arg/HA-SA presented more mineralized nodule formation compared with other groups (**Figure 4B and D**). To further explore the osteogenesis of the rBMSCs inside the microspheres, we adopted the immunofluorescence staining of osteogenesis genes including collgen-1 (Col-1) and osteocalcin (OCN) of the rBMSC laden microspheres. We found 1% Arg/HA-SA group showed significantly higher fluorescence staining intensity of Col-1 and OCN on day 3 and 7 respectively, indicating the Arg/HA loading could provide a favorable osteogenic microenvironment and enhance the osteogenic differentiation of rBMSCs (**Figure 4E, F and Figure S4**). We additionally used quantitative real-time reverse transcription PCR (qRT-PCR) to characterize the relative expression of osteogenesis genes Col-1, OCN, and bone morphogenetic protein-2 (BMP-2) on day 1, 3, 7 and 14. We found that the Arg/HA group could promote the expression of all selected osteogenic genes, exhibiting superior performance

in osteogenic differentiation of rBMSCs inside the microspheres (**Figure 4G to I**). The above results indicated that the Arg/HA loading could provide a favorable osteogenic microenvironment and enhance the osteogenic differentiation of rBMSCs.

To evaluate the mechanism of regulating the osteogenic differentiation, we assessed the NO generation and activation status of the NO/cGMP signalling pathway of the encapsulated rBMSCs. As expected, the presence of Ca^{2+} in HA/SA and Arg-HA/SA groups could significantly enhance the expression of endothelial nitric oxide synthase (eNOS) in rBMSCs, which indicated that the Ca^{2+} up-regulated the activity of eNOS (**Figure 4J**). The NO production characterized by nitrite concentration with Griess reagent method also revealed the synergic promotion of NO generation by released Ca^{2+} and L-arginine since the Arg-HA/SA showed the most significantly increased NO production (**Figure 4K**). Finally, we quantified the cGMP expression by ELISA kit and found that the Arg-HA/SA groups presented the highest cGMP concentration, indicating the activation of NO/cGMP signalling pathway (**Figure 4L**).

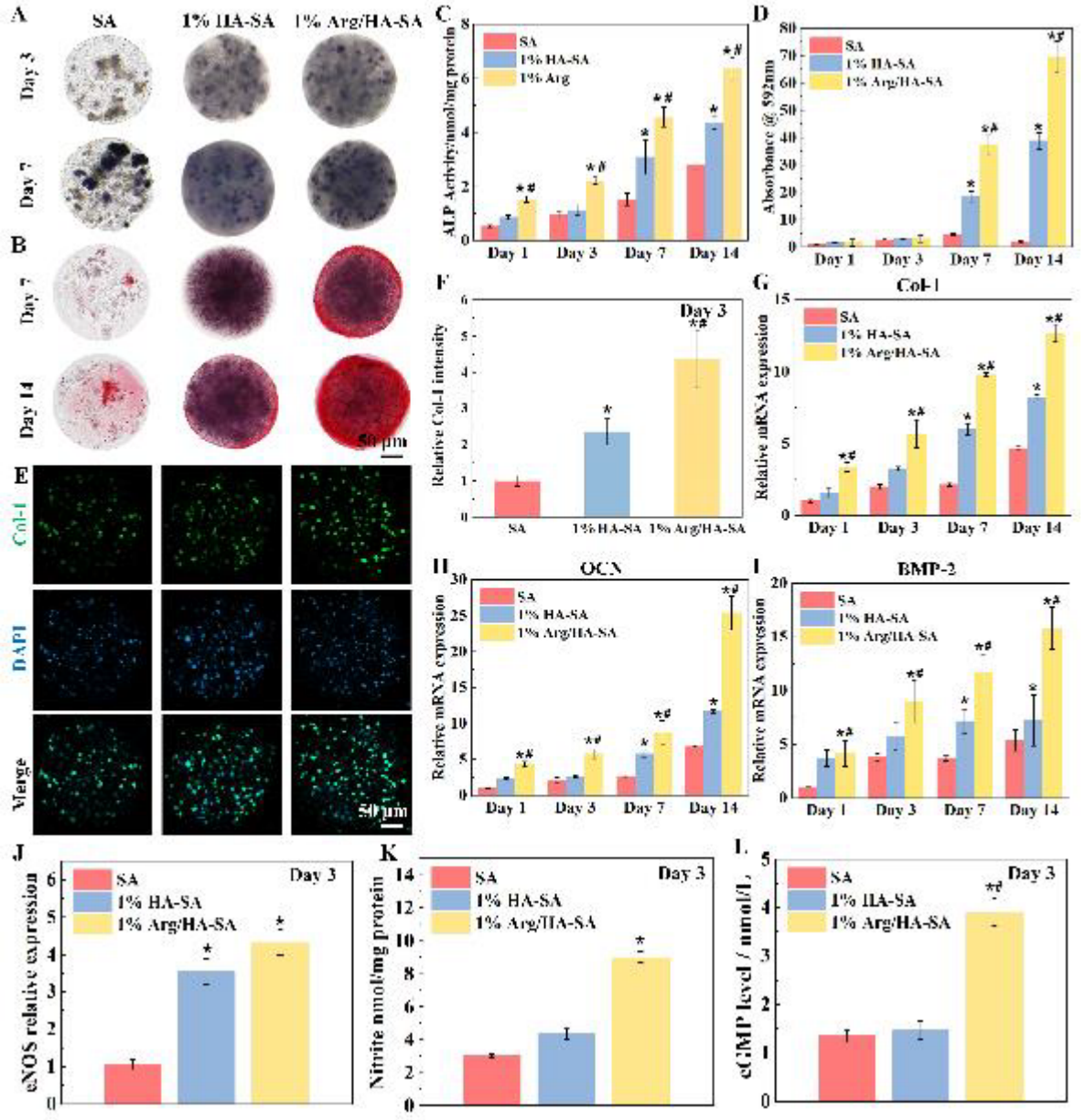

Figure 4. *In vitro* osteogenesis characterization of rBMSCs inside regeneration-enhancer-element microspheres. (A) ALP staining of the rBMSC encapsulated microspheres on day 3 and 7 and (B) ARS staining of the rBMSC encapsulated microspheres on day 7 and 14. (C) Quantification of ALP activity on day 1, 3, 7 and 14 and (D) quantification of ARS assay on day 1, 3, 7 and 14. (E) Col-1 staining and (F) relative fluorescence intensity of the rBMSC encapsulated microspheres on day 3; (G to I) Relative mRNA expression of osteogenic genes of rBMSCs (Col-1, OCN and BMP-2) on day 1, 3, 7 and 14. (J) Relative eNOS expression, (K) NO generation and (L) cGMP expression of rBMSCs inside different microspheres. NO was indicated by nitrite levels and cGMP concentration was evaluated by ELISA. Sample size n =

3 for all experiments. Data are analyzed by a two-way ANOVA with a Tukey's post hoc test for multiple comparison. Data are presented as mean ± SD. *$p < 0.05$ and $^{\#}p < 0.05$ are considered significantly different compared with the SA group and the 1% HA-SA group respectively.

Other than the osteogenic promotion of rBMSCs inside the microspheres, we also hypothesized such regeneration-enhancer-element reservoirs could power the osteogenesis-angiogenesis coupling of the surrounding rBMSCs and ECs due to the diffusion of generated NO, Ca^{2+} and L-arginine. We thus evaluated the enhancement effect of different microspheres on the osteogenesis of rBMSCs and angiogenesis of HUVECs outside the microspheres through co-culture experiments (**Figure 5A**). The pure SA microspheres, the SA microspheres encapsulating Arg/HA (Arg/HA-SA) and the SA microspheres encapsulating rBMSCs and Arg/HA (Arg/HA-SA@BMSC) were adopted in this study. In the co-culture of rBMSCs with microspheres, we found that the Arg/HA-SA@BMSC groups demonstrated higher ALP activity and matrix mineralization than other groups both in staining and quantification assay (**Figure 5B, C, F and G**). The heightened expression of osteogenic genes (Col-1, OCN and BMP-2) on day 7 also demonstrated the enhanced osteogenic differentiation of rBMSCs co-cultured with Arg/HA-SA@BMSC (**Figure 5H**). We additionally performed the Col-1 and OCN immunofluorescence staining of the rBMSCs outside the microspheres on day 3 and 7 and found that the Arg/HA-SA@BMSC group presented the highest florescence intensity of both Col-1 and OCN, indicating the Arg/HA-SA@BMSC microspheres could promote the ECM deposition of osteoblasts (**Figure S5**). Next, we co-cultured the HUVECs with the same formulation of microspheres. We found that the Arg/HA-SA@BMSC groups demonstrated the largest CD31 (an angiogenic formation marker)-positive staining area (**Figure 5D**). The quantification of CD31 intensity also revealed 5.25 fold and 1.55 fold increase of Arg/HA-SA@BMSC groups compared to the SA and HA-SA groups (**Figure S6**). To further evaluate

the angiogenic potential of our microspheres, we performed the wound closure assay and found that the wound closure rate of Arg/HA-SA@BMSC group was significantly elevated compared to other groups, indicating the improved migration of HUVECs which could contribute to enhanced angiogenesis (**Figure S7A and B**). Moreover, in the tube formation assay, we found that the Arg/HA-SA@BMSC group could significantly enhance the tubulogenesis of HUVECs with the longest average tube length of 49.36 ± 3.71 mm, as well as the most branching points of 89 ± 5.5 at 8 h (**Figure 5E, I** and **Figure S8**). Additionally, the angiogenic gene expression of CD31, vascular endothelial growth factor A (VEGF-A) and angiopoietin 1 (Ang-1) in the Arg/HA-SA@BMSC group was also the highest on day 3 (**Figure 5J**). All in all, the above results collectively presented facile osteogenesis and angiogenesis coupling of rBMSCs and HUVECs resulting from the co-culture with Arg/HA-SA@BMSC microspheres.

To confirm the activation of NO/cGMP signalling pathway in the presence of released Ca^{2+} and L-arginine, we evaluated the key parameters in the NO/cGMP signalling pathway of both rBMSCs and HUVECs. We found that the Arg/HA-SA and Arg/HA-SA@BMSC group presented nearly 2.52 fold and 3.06 fold increase in the eNOS activity for rBMSCs and 5.24 fold and 6.18 fold increase for HUVECs compared to their respective SA groups (**Figure 5K**). In the analysis of nitrite concentration and cGMP levels, we found that the Arg/HA-SA@BMSC group showed the highest nitrite concentration and cGMP levels with upregulated NO/cGMP signaling pathway for both cells (**Figure 5L** and **M**). This is due to the stimulation of the NO release from the rBMSCs inside the microspheres and NO production by external cells by Ca^{2+} and L-arginine. Conclusively, the above results demonstrated that the Arg/HA-SA@BMSC microspheres could promote the osteogenesis and angiogenesis coupling of externally co-cultured rBMSCs and HUVECs through the coordinated activation of NO/cGMP signalling pathway.

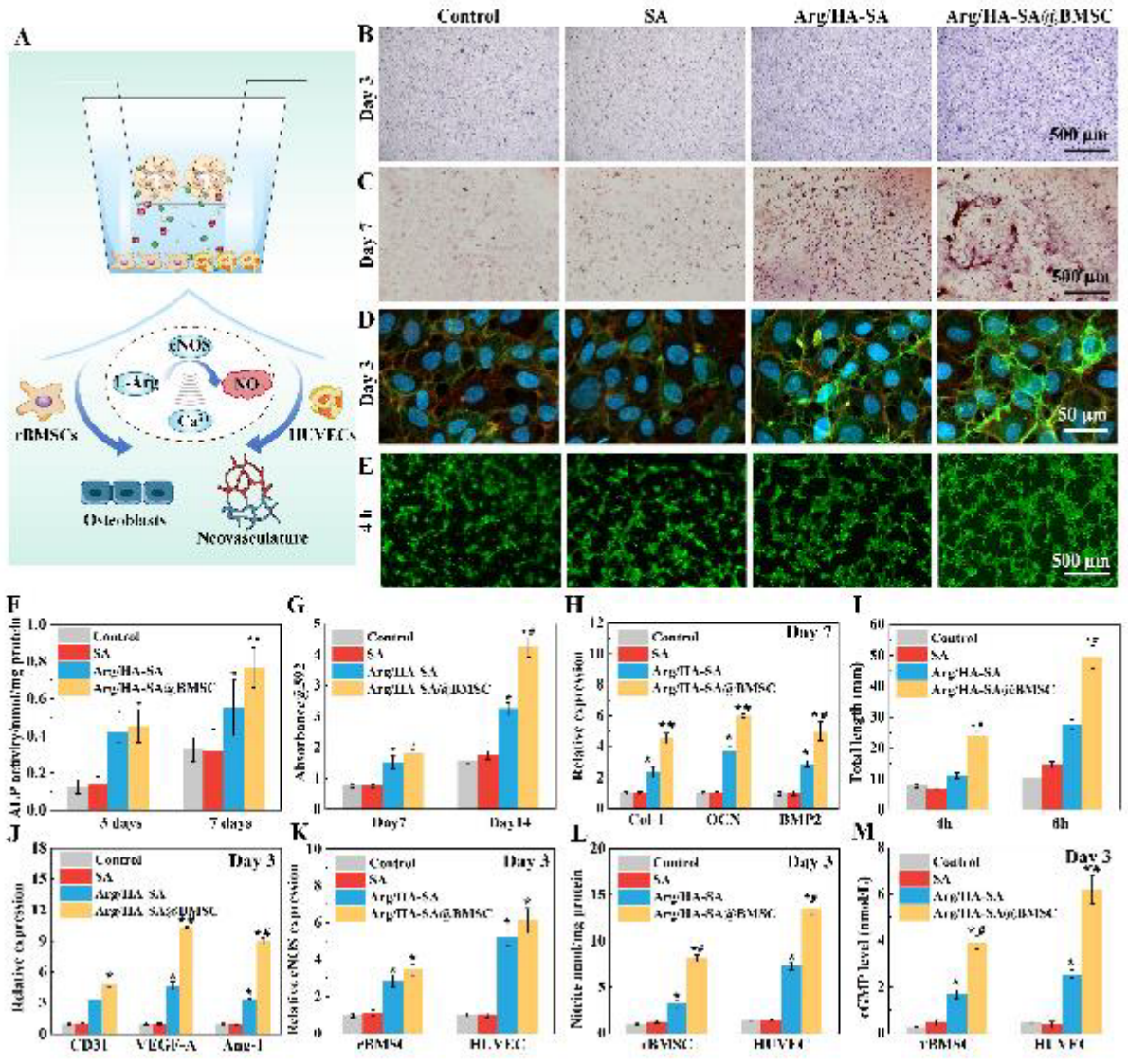

Figure 5. *In vitro* evaluation of osteogenesis and angiogenesis coupling of rBMSCs and HUVECs outside the microspheres. (A) Schematic diagram of the co-culture assay of rBMSCs and HUVECs with the microspheres. (B) ALP and (C) ARS staining of the rBMSCs co-cultured with the microspheres on day 3 and 7 respectively. (D) Representative CD31 immunofluorescence staining on day 3 and (E) formation of tubular network of HUVECs co-cultured with different microspheres after 4 h. Quantification of (F) ALP activity, (G) mineralization and (H) relative expression of osteogenic genes (Col-1, OCN and BMP-2) of rBMSCs in the co-culture assay on day 7. (I) Quantification of the tube formation assay and (J) relative expression of angiogenic genes (CD31, VEGF-A and Ang-1) of HUVECs in the co-culture assay on day 3. (K) Relative eNOS expression, (L) nitrite levels and (M) cGMP

concentration of rBMSCs and HUVECs on day 3. Sample size $n = 3$ for all experiments. Data are analyzed by a two-way ANOVA with a Tukey's post hoc test for multiple comparison. Data are presented as mean ± SD. $^{*}p < 0.05$ and $^{\#}p < 0.05$ are considered significantly different compared with the SA group and the Arg/HA-SA group respectively.

While previous evaluation demonstrated the effectiveness of our regeneration-enhancer-element reservoirs (Arg/HA-SA@BMSC) to promote osteogenesis and angiogenesis *in vitro*, their clinical therapeutic efficacy was still unexplored. We hence proceeded to evaluate the bone regeneration potential of our regeneration-enhancer-element reservoirs *in vivo* with rat critical-sized calvarial defect model (**Figure 6B**). Four groups were adopted in total: the pure SA microspheres without rBMSC encapsulation (SA), the Arg-HA/SA microspheres without rBMSC encapsulation (Arg/HA-SA), the Arg-HA/SA microspheres with rBMSC encapsulation (Arg/HA-SA@BMSC), and the untreated groups (blank, control). To evaluate the immune response of the microspheres after implantation, we first performed the immunofluorescence staining of proinflammatory cytokines including interleukin 6 (IL-6) and tumor necrosis factor alpha (TNF-α). We found that all groups showed little IL-6 and TNF-α infiltration, indicating that the cell-laden microspheres elicit no detrimental effect on the bone regeneration process (**Figure S9**). Micro-CT scanning and reconstruction was used to assess the new bone formation after 4- and 8-week implantation. We observed newly formed bone tissues in all implantation groups and the Arg/HA-SA@BMSC group showed the largest area of new bone tissues among all groups (**Figure 6A**). In the analysis of bone mineral density (BMD) and bone tissue volume/total tissue volume (BV/TV), the Arg/HA-SA@BMSC group demonstrated 2.19 fold increase of BMD and 3.6 fold increase of BV/TV compared to the SA group after 8 weeks (**Figure 6C an D**). The histological analysis of hematoxylin and eosin (H&E) and Masson's trichrome staining were further adopted to evaluate the new bone reconstruction in the defect site. In H&E staining, we found the blank and SA groups presented most fibrous tissues with

limited bone formation, while the Arg/HA-SA@BMSC group showed obvious woven and lamellar bone tissues after 4-week implantation (**Figure S10**). Meanwhile, in the Masson's trichrome staining, we could observe more mature lamellar bone (red staining) in the Arg/HA-SA@BMSC groups with 3.15 fold and 1.58 fold increase compared to SA and Arg-HA/SA groups after 8-week implantation (**Figure S11**). All these results indicated our regeneration-enhancer-element reservoirs (Arg/HA-SA@BMSC) could significantly power new bone formation in the defect site.

To further validate the osteogenesis and angiogenesis coupling of the enhancer-element reservoirs, we performed the immunofluorescence staining of CD31 and OCN as angiogenesis and osteogenesis marker respectively. We found that the newly formed bone tissues (OCN, green staining) were located around the neo-vascular regions (CD31, red staining), indicating that the neo-vasculature could support the bone regeneration process. The Arg/HA-SA and Arg/HA-SA@BMSC groups presented more CD31 and OCN stained cells in the defect site, indicating their superior potential to promote the osteogenesis and angiogenesis coupling (**Figure 7A**). Quantitatively, the Arg/HA-SA@BMSC group also presented significantly increased vascular numbers and OCN intensity compared to the Arg/HA-SA groups 8 weeks post-operation (**Figure 7B** and **C**). This is attributed to the promotion of osteogenesis and angiogenesis by enhancement elements in the Arg/HA-SA@BMSC groups (NO, Ca^{2+} and L-arginine) during bone regeneration. Altogether, through coupling the osteogenesis and angiogenesis and the interaction of the inside/outside cells, our Arg/HA-SA@BMSC microspheres may direct the future clinical invasive therapy for vascularized bone regeneration.

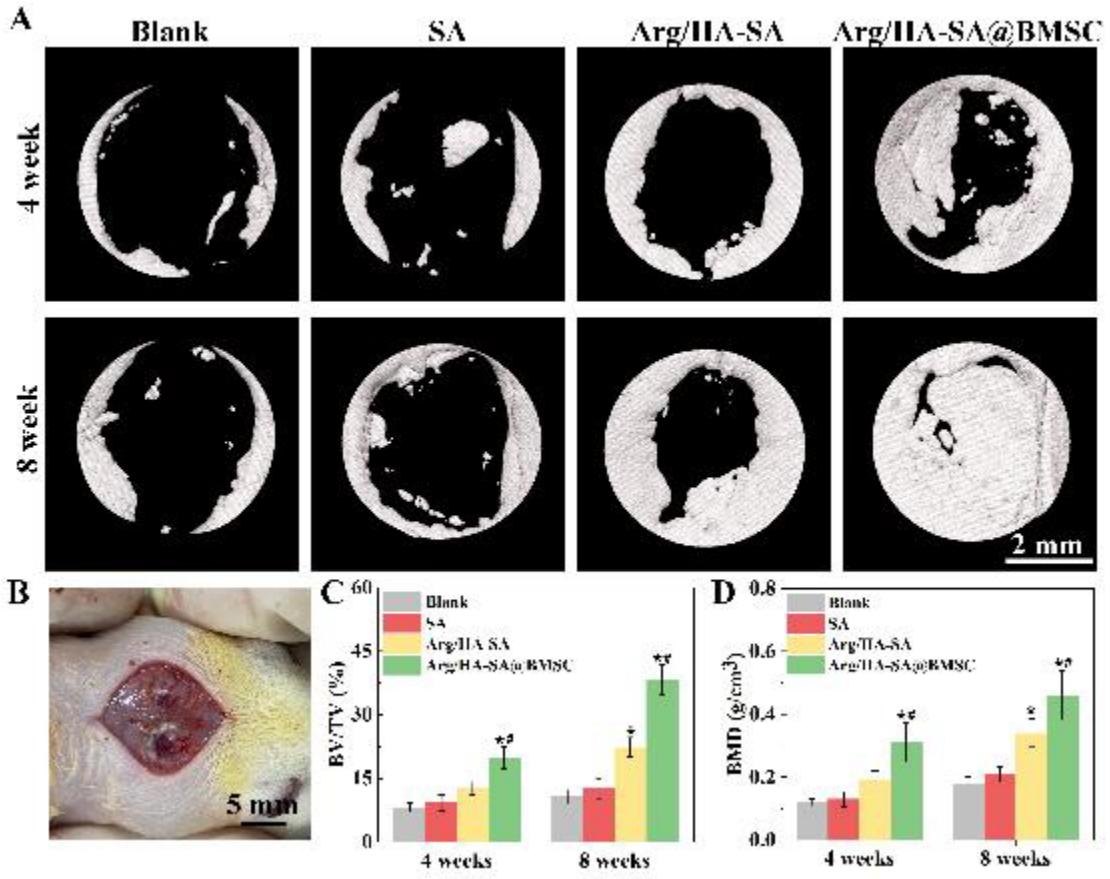

Figure 6. *In vivo* bone regeneration efficacy of different microspheres. (A) Micro-CT scanning of newly formed bone tissue 4- and 8-week post implantation. (B) The critical-sized calvarial defect model with two round defects was created for the bone regeneration evaluation. Quantitative evaluation of (C) BMD and (D) BV/TV of new bone formation 4- and 8-week post implantation. Sample size $n = 6$ for all experiments. Data are analyzed by a two-way ANOVA with a Tukey's post hoc test for multiple comparison. Data are presented as mean ± SD. *$p < 0.05$ and $^{\#}p < 0.05$ are considered significantly different compared with the SA group and the Arg/HA-SA group respectively.

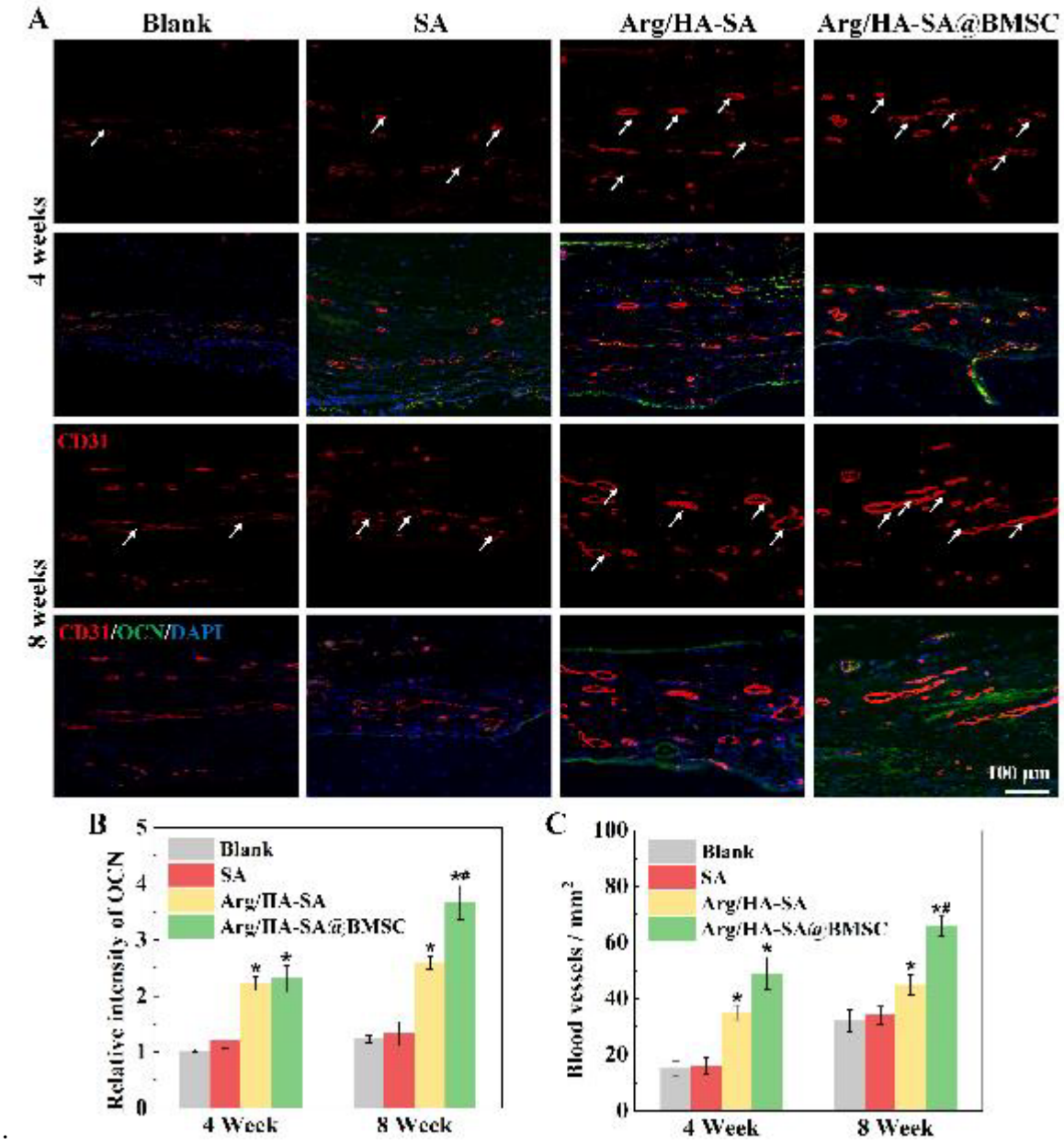

Figure 7. *In vivo* histology analysis of different microspheres. (A) CD31 and OCN immunofluorescence staining at 4 and 8 weeks. The red and green fluorescence denote the CD31 and OCN positive cells respectively and white arrows indicate the neovascular site. Quantification of (B) relative OCN intensity and (C) blood vessel numbers. Sample size $n = 6$ for all experiment. Data are analyzed by a two-way ANOVA with a Tukey's post hoc test for multiple comparison. Data are presented as mean ± SD. $^{*}p < 0.05$ and $^{\#}p < 0.05$ are considered significantly different compared with the SA group and the Arg/HA-SA group respectively.

3. Conclusion

To conclude, we have electrosprayed rBMSC-laden Arg/HA-SA microspheres as a regeneration-enhancer-element reservoir (Arg/HA-SA@BMSC) for bone regeneration. The enhancer elements Ca^{2+} and L-arginine are sustainably released from the doped nanoparticles, while NO is generated by encapsulated BMSCs via eNOS. The Arg/HA-SA@BMSC display enhanced osteogenesis and angiogenesis coupling by activating the NO/cGMP signalling pathway for both encapsulated rBMSCs and externally co-cultured HUVECs and rBMSCs, as well as significantly increased bone tissue formation around neovasculature in rat calvarial defect model. Together, our microspheric reservoirs could stimulate regeneration via an internal/external modulation loop of encapsulated cells and native cells at the defect site, bringing forth a novel interpretation for minimally invasive treatment for bone fractures.

4. Experimental Section

Synthesis of Arg-HA NPs: The Arg/HA NPs were synthesized through hydrothermal method according to previous research.[19] Briefly, 100 mL 0.5 M calcium nitrate ($Ca(NO_3)_2$ $4H_2O$) (Macklin, China) was added dropwisely in 150 mL 0.05 M ammonium dibasic phosphate ($(NH_4)_2HPO_4$)) (Macklin, China) solution supplemented with different concentration of L-arginine (0.01 M, 0.05 M, 0.1 M, Macklin, China). The reaction was kept at 60 ºC and pH 12 for 24 hours. After the reaction was complete, Arg/HA NPs was collected by centrifugation under 10,000 r/min for 10 minutes, followed by filtration and washing. Finally, the precipitated Arg/HA NPs was dried overnight under vacuum.

Characterization of the Arg-HA NPs: TEM (Tecnai F20, Netherlands) was adopted to evaluate the morphology of the prepared Arg/HA NPs.[16] The Arg-HA NPs was dispersed in dichloromethane (DCM, Macklin, China) (0.2 g/L), followed by 10 minute sonication. Then, the suspension was dropped onto the copper grid and air dried. ATR-FTIR was additionally

used to characterize the Arg/HA with the range of wavelength set at 650-4000 cm^{-1}, 2 cm^{-1} resolution.[20] We then evaluated the crystal structure of the Arg/HA NPs by XRD (Bruker, US) with 0.05°/s scanning rate.[21] The patterns were analyzed by the standard card of HA (JCPDS No. 09-432). DLS (Malvern, UK) was used for testing equivalent average hydrodynamic diameter of Arg/HA with glass cuvette at 25ºC.[22]

Evaluation of L-arginine and calcium ion (Ca^{2+}) release: L-arginine and Ca^{2+} release profiles from Arg/HA NPs were measured by soaking the NPs (10 mg) into 2 mL Ca^{2+}/Mg^{2+}-free phosphate-buffered saline (PBS) at 37°C for 4 weeks. For each predetermined time point, 50 μL supernatant was used for analysis, and an equal volume of fresh PBS was added for continuing the test. The total concentration of L-arginine was tested by high performance liquid chromatography (HPLC, Hitachi L-2000, Japan) while the Ca^{2+} release was detected using inductive coupled plasma optical emission spectrometer (ICP-OES, Thermo Scientific, Hong Kong).[13]

Preparation of Arg/HA-SA microspheres: Arg/HA-SA microspheres were prepared by electrospraying according to former protocols.[23] Briefly, 100 mg SA (Macklin, China) supplemented with 0.5%, 1%, 2% (w/w) Arg/HA was suspended in 10 mL distill water, followed by 12 hours of stirring to form a homogenous suspension. For cell-laden samples, 1×10^8 cells were suspended in the mixture with the final cell density of 1×10^7 cells/mL. The mixture was then loaded into a plastic syringe as an electrospray solution. A collecting bath containing 0.5 M $CaCl_2$ (Macklin, China) was placed 6 cm below the nozzle. The nozzle and the collector were connected to high-voltage power of 5 kV and -2 kV respectively. The electrospray speed was set at 1 mL/h. After electrospray, the prepared microspheres were washed with PBS and transferred for further incubation. The morphology of the microspheres was visualized by an inverted microscope (Nikon, Japan) and the diameter of the microspheres

was analyzed by the Image J software (NIH, USA).[24] Microcompresseion test was performed using TA.XT Plus texture analyser (Stable Micro Systems, UK) to derermine the Young's modulus of the micropheres as previouly described.[25] Brefliy, the micropheres were placed on the glass chamber and compressed at 5 μm/s until 25% strain. The force and displacement curves were recorded and the Young's modulus was caculated according to the Hertz model: $E = \frac{3(1-v^2)}{4R^{1/2}} \frac{F}{(H/2)^{3/2}}$, where E was the Young's modulus, F was the applied force, R was the initial radius of the micropheres, H was the deformation and v is the Poisson's ratio of the alginate (set as 0.5 according to the previsou work[26]). Three samples were tested for statistical analysis. The degradation of microspheres was evaluated by immersing the microspheres in PBS for 28 days. At predetermined time points, we observed the morphology change of the microspheres by an inverted microscope.

In vitro cell encapsulation characterization: rBMSCs (Cyagen, Hong Kong) were adopted to evaluate the cell survival and proliferation in the electrosprayed microspheres. After fabrication of rBMSC-laden microspheres, they were incubated in α minimal essential medium (α MEM, Thermo Fisher, China) with addition of 10% fetal bovine serum (FBS) and 1% Penicillin-Streptomycin (P/S). We then performed Live/Dead assay (Beyotime, China) and PicoGreen assay (Solarbio, China) to evaluate the cell viability and cell proliferation respectively after 1, 3 and 7 days of culture according to the previous protocols.[27] Quantification of cell viability equals to the ratio between live cells and total cells.[1] In addition, the cell release density was evaluated according to literature.[28] Briefly, the cell laden microspheres were firstly resuspended with culture medium and cultured in a 24-well flask. At predetermined time points of day 1, 14, 21 and 28, the cells released from the microspheres were observed by an inverted microscope and the cell release density per unit area was quantified by dividing the released cell number with the image area in six randomized images using Image J software.

In vitro osteogenesis characterization of rBMSCs encapsulated in microspheres: rBMSC laden microspheres were cultured in osteogenic medium (Cyagen, China). On day 3 and 7, the ALP staining kit (Beyotime, China) was adopted to detect the ALP activity based on the manufacturer's protocol. ALP quantification kit (Beyotime, China) was performed on day 1, 3 ,7 and 14 to quantify the ALP activity. Furthermore, the relative expression of osteogenic genes including Col-1, OCN and BMP-2 were evaluated by qRT-PCR on day 1, 3, 7 and 14.[13] In addition, ARS staining (Solarbio, China) was used to assess the mineralized matrix formation in the cell-laden microspheres after 1, 3, 7 and 14 days incubation following our previously protocol.[29] Moreover, Col-1 and OCN immunofluorescence staining was adopted on day 3 and 7. Briefly, the rBMSC-laden microspheres were fixed by 4% paraformaldehyde (Bioshark, China) for 15 min. After wash by PBS, the microspheres were permeabilize by 0.2% Triton X-100 (Beyotime, China) and blocked by 1% BSA solution (Beyotime, China). Microspheres were incubated with diluted Col-1 (1:250, Abcam, UK) and OCN (1:400, Bioss, China) primary antibody overnight at 4°C. Here, we used Alexa Fluor-coupled secondary antibodies (Abcam, UK) and captured images by a confocal laser scanning microscope (Zeiss, German). Furthermore, the relative expression of osteogenic genes including Col-1, OCN and BMP-2 was evaluated by qRT-PCR after 1, 3, 7 and 14 days.[16] Briefly, after total RNA extraction (OMEGA Bio-tek, USA) and reverse-transcription (Takara, China), we performed the Real-time PCR using CFX96 Touch (Bio-rad, USA). GAPDH was used for normalization and the primer sequences utilized were listed in Table S1.

In vitro osteogenesis and angiogenesis characterization of rBMSCS and *HUVECs surrounding the microspheres*: The effect of the prepared microspheres on osteogenesis of rBMSCs and angiogenesis of HUVECs were evaluated via a transwell based co-culture system. In detail, for the osteogenesis of rBMSCs, 2×10^4 cells/cm^2 rBMSCs were seeded in the bottom well of the transwell plate (Corning, USA) in osteogenic medium (Cyagen, China). We first prepared the

osteogenic meidum containing high concentration of micropheres and dropped 100 μL microsphere suspension onto the glass sides. The number of the micropheres was then counted under a microscope. By adjusting the microphere concentration, 100 microspheres in 200 μL osteogenic medium was eventually added in the upper chamber of the transwell. Similarly, for angiogenesis of HUVECs, 4×10^4 cells/cm^2 HUVECs were seeded in the bottom well of the transwell culture plate in endothelial cell medium (ECM, Sciencell, USA) and 100 microspheres was cultured in the upper chamber of the transwell.[22] The osteogenic differentiation experiments and fluorescence staining of Col-1 and OCN of rBMSCs were also performed with the aforementioned method on day 7. For the angiogenesis analysis, we performed the CD31 immunofluorescence staining after 3 days of incubation. Briefly, cells were fixed with 4% paraformaldehyde (Bioshark, China) for 10 minutes and submerged in 0.2% (v/v) Triton X-100 (Beyotime, China) for 15 minutes to increase the permeability. After incubation with blocking buffer (Beyotime, China), the cells were incubated with the CD31 primary antibodies (Abcam, UK) and washed with PBS. Here, we used Alexa Fluor-coupled secondary antibodies (Abcam, UK) and captured images by and inverted fluorescence microscope (Nikon, Japan). Wound closure assay of HUVECs was conducted according to previously reported protocol.[30] Briefly, 5×10^5 cells/cm^2 HUVECs were seeded in 6-well plates. After cell confluence, 200 μL pipette tip was used to scratch the cell layer. Inverted microscope was then used to observe the wound closure status at 0 and 24 h. The image J software was used to quantify the wound closure rate. Then, we conducted the tube formation assay of HUVECs. Briefly, 5×10^4 cells/cm^2 HUVECs were seeded onto the surface of the Matrigel coated 24-well plate to allow the tube formation.[31] After 4 and 8 hours, HUVECs were stained with Calcein AM (Thermo Fisher, Hong Kong) and photographed by a fluorescence microscope (Nikon, Japan). The parameters of tube formation including total branch length and average number of junctions were quantified in five random fields using

Image J software. Besides, the expressions of CD31, VEGF-A and Ang-1 on day 3 was also evaluated through qRT-PCR. The primer sequences utilized were listed in **Table S1**.

Mechanism elucidation of NO/cGMP signaling pathway: To evaluate the expression of key signaling molecules in NO/cGMP signalling pathway, we applied the qRT-PCR to quantify the eNOS gene expression for rBMSCs encapsulated in the microspheres or rBMSCs/HUVECs surrounding the microspheres on day 3. The NO production was evaluated by measuring the concentration of nitrite using the Griess method.[29] Briefly, after 3 days of incubation, the nitrite concentration in the culture supernatants of both cells was quantified using Total Nitric Oxide Assay (Beyotime, China) following the manufacturer's protocol.[32] The level of cGMP was additionally assessed by the cGMP ELISA kit on day 3 (Bioss, China).

In vivo bone repair evaluation: Critical-sized calvarial defect model was adopted for *in vivo* bone repair evaluation with Sprague-Dawley rats (male, approximately 250 g) with the permission from the Ethics Committee of the Hong Kong Polytechnic University (Ref No. 19-20/65-BME-R-GRF).[13, 33] Briefly, the rats were injected with pentobarbital sodium solution (30–40 mg/kg body weight) for anesthetization. Then, we created a sagittal incision on the skull and made two 5-mm sized defects. The defects were then injected with 100 microspheres in 50 μL normal saline of different groups or left blank. Finally, the defect sites were closed with victory resorbable sutures (4-0) and the animals were housed in separate cages after the surgery and supplemented with free soft food and water. After 4 and 8 weeks of implantation, the rats were euthanized by CO_2 asphyxiation and the skull tissues were obtained and fixed in 10% neutral buffered formalin for the following evaluations. The micro-CT (SkyScan, Belgium) was used to analyze the bone regeneration in the implantation area.[33] BMD and BV/TV were conducted by the CT-analyzer software, according to the previous method.[13] Then, the harvested skull tissues were decalcified for histological evaluation. The H&E and Masson's

trichrome staining was used to assess the new bone formation.[34] The CD31 and OCN immunohistochemical staining (Abcam, UK) was also performed to analyze the osteogenesis-angiogenesis coupling effect in the regeneration sites according to the literature.[34] Meanwhile, the IL-6 and TNF-α immunofluorescence staining (Servicebio, China) was performed to evaluate the immune response of the microspheres after implantation according to the literature.[35]

Statistical analysis: All results are presented as the mean values ± standard deviation (SD). One-way or two-way analysis of variance (ANOVA) followed by Tukey's multiple comparison test (GraphPad Prism 8, USA) was conducted and p-value < 0.05 was considered statistically significantly different.

Supporting Information

Supporting Information is available from the Wiley Online Library or from the author.

Acknowledgements

T. Xu. and Y. Yang. contributed equally to this work. This work was supported by the Excellent Young Scholars Projects from the National Science Foundation of China (82122002) and intra-faculty fund (ZVPC) from The Hong Kong Polytechnic University.

Received: ((will be filled in by the editorial staff))

Revised: ((will be filled in by the editorial staff))

Published online: ((will be filled in by the editorial staff))

References

[1] X. Zhao, S. Liu, L. Yildirimer, H. Zhao, R. H. Ding, H. N. Wang, W. G. Cui, D. Weitz, *Advanced Functional Materials* **2016**, *26* (17), 2809.

[2] Y. Li, W. Liu, F. Liu, Y. Zeng, S. Zuo, S. Feng, C. Qi, B. Wang, X. Yan, A. Khademhosseini, J. Bai, Y. Du, *Proc. Natl. Acad. Sci. U. S. A.* **2014**, *111* (37), 13511.
[3] a) Z. Zhang, M. J. Gupte, X. Jin, P. X. Ma, *Adv. Funct. Mater.* **2015**, *25* (3), 350; b) H. Zhao, J. H. Xu, W. J. Lan, T. Wang, G. S. Luo, *Chem. Eng. J.* **2013**, *229*, 82.
[4] a) W. Leong, D. A. Wang, *Trends Biotechnol.* **2015**, *33* (11), 653; b) X. H. Liu, X. B. Jin, P. X. Ma, *Nat. Mater.* **2011**, *10* (5), 398; c) Z. Y. Zhao, Z. Wang, G. Li, Z. W. Cai, J. Z. Wu, L. Wang, L. F. Deng, M. Cai, W. G. Cui, *Adv. Funct. Mater.* **2021**, *31* (31), 2103339.
[5] a) Y. Y. Yang, T. S. Chung, N. P. Ng, *Biomaterials* **2001**, *22* (3), 231; b) T. W. King, C. W. Patrick, *J. Biomed. Mater. Res.* **2000**, *51* (3), 383.
[6] J. Z. Wu, G. Li, T. J. Ye, G. H. Lu, R. M. Li, L. F. Deng, L. Wang, M. Cai, W. G. Cui, *Chem. Eng. J.* **2020**, *393*, 124715.
[7] D. Wu, Y. Yu, C. Zhao, X. Shou, Y. Piao, X. Zhao, Y. Zhao, S. Wang, *ACS Appl. Mater. Interfaces* **2019**, *11* (37), 33716.
[8] Z. Jiang, B. Xia, R. McBride, J. Oakey, *J. Mater. Chem. B* **2017**, *5* (1), 173.
[9] J. N. Etter, M. Karasinski, J. Ware, R. A. Oldinski, *J. Mater. Sci. Mater. Med.* **2018**, *29* (9), 143.
[10] A. Moshaverinia, C. Chen, K. Akiyama, S. Ansari, X. T. Xu, W. W. Chee, S. R. Schricker, S. T. Shi, *J. Mater. Sci. Mater. Med.* **2012**, *23* (12), 3041.
[11] J. Kim, H. N. Kim, K. T. Lim, Y. Kim, S. Pandey, P. Garg, Y. H. Choung, P. H. Choung, K. Y. Suh, J. H. Chung, *Biomaterials* **2013**, *34* (30), 7257.
[12] L. B. Zhao, L. Pan, K. Zhang, S. S. Guo, W. Liu, Y. Wang, Y. Chen, X. Z. Zhao, H. L. Chan, *Lab Chip* **2009**, *9* (20), 2981.
[13] Y. Yang, T. Xu, Q. Zhang, Y. Piao, H. P. Bei, X. Zhao, *Small* **2021**, *17* (14), e2006598.
[14] W. Pan, L. D. Quarles, L. H. Song, Y. H. Yu, C. Jiao, H. B. Tang, C. H. Jiang, H. W. Deng, Y. J. Li, H. H. Zhou, Z. S. Xiao, *J. Cell. Biochem.* **2005**, *94* (2), 307.
[15] B. Jogiya, K. Chudasama, V. Thaker, M. Joshi, *J. Nanomed. Res.* **2016**, *3* (6), 00073.
[16] Y. Yang, Q. Zhang, T. Xu, H. Zhang, M. Zhang, L. Lu, Y. Hao, J. H. Fuh, X. Zhao, *Biomaterials* **2020**, *263*, 120378.
[17] H. K. Koerten, J. van der Meulen, *J. Biomed. Mater. Res.* **1999**, *44* (1), 78.
[18] a) S. S. Ho, A. T. Keown, B. Addison, J. K. Leach, *Biomacromolecules* **2017**, *18* (12), 4331; b) A. Lueckgen, D. S. Garske, A. Ellinghaus, D. J. Mooney, G. N. Duda, A. Cipitria, *Biomaterials* **2019**, *217*, 119294.
[19] Y. Z. Zhao, J. Zhu, S. H. Zhu, Y. Y. Huang, Z. Y. Li, K. C. Zhou, *Trans. Nonferrous Met. Soc.* **2011**, *21* (8), 1773.
[20] V. Bunpetch, Z. Y. Zhang, X. Zhang, S. Han, P. Zongyou, H. Wu, O. Hong-Wei, *Biomaterials* **2019**, *196*, 67.
[21] L. Melly, G. Cerino, A. Frobert, S. Cook, M. N. Giraud, T. Carrel, H. T. Tevaearai Stahel, F. Eckstein, B. Rondelet, A. Marsano, A. Banfi, *J. Cell. Mol. Med.* **2018**, *22* (5), 2580.
[22] H. W. Cheng, K. D. Luk, K. M. Cheung, B. P. Chan, *Biomaterials* **2011**, *32* (6), 1526.
[23] Y. Xu, J. Peng, G. Richards, S. Lu, D. Eglin, *J. Orthop. Transl.* **2019**, *18*, 128.
[24] H. Liu, Z. Cai, F. Wang, L. Hong, L. Deng, J. Zhong, Z. Wang, W. Cui, *Adv. Sci.* **2021**, *8* (18), e2101619.
[25] a) M. Yuan, X. J. Ju, R. Xie, W. Wang, L. Y. Chu, *Particuology* **2015**, *19*, 164; b) I. Zafeiri, A. Beri, B. Linter, I. Norton, *Carbohydr. Polym.* **2021**, *255*, 117373.
[26] C. Wang, C. Cowen, Z. Zhang, C. R. Thomas, *Chem. Eng. Sci.* **2005**, *60* (23), 6649.
[27] X. Zhao, X. Sun, L. Yildirimer, Q. Lang, Z. Y. W. Lin, R. Zheng, Y. Zhang, W. Cui, N. Annabi, A. Khademhosseini, *Acta Biomater.* **2017**, *49*, 66.
[28] Y. C. Xu, Y. Gu, F. Cai, K. Xi, T. W. Xin, J. C. Tang, L. Wu, Z. Wang, F. Wang, L. F. Deng, C. P. Leite, B. Sarmento, W. G. Cui, L. Chen, *Adv. Funct. Mater.* **2020**, *30* (52), 2006333.
[29] A. Oryan, A. Kamali, A. Moshiri, M. B. Eslaminejad, *Cells Tissues Organs* **2017**, *204* (2), 59.

[30] N. Jabbari, M. Nawaz, J. Rezaie, *Cell Commun. Signal.* **2019**, *17* (1), 165.
[31] Y. H. Choi, S. C. Heo, Y. W. Kwon, H. D. Kim, S. H. Kim, I. H. Jang, J. H. Kim, N. S. Hwang, *Acta Biomater.* **2015**, *25*, 76.
[32] C. Sonnet, C. L. Simpson, R. M. Olabisi, K. Sullivan, Z. Lazard, Z. Gugala, J. F. Peroni, J. M. Weh, A. R. Davis, J. L. West, E. A. Olmsted-Davis, *J. Orthop. Res.* **2013**, *31* (10), 1597.
[33] P. F. Wei, Z. Y. Yuan, W. Jing, B. B. Guan, Z. H. Liu, X. Zhang, J. P. Mao, D. F. Chen, Q. Cai, X. P. Yang, *Biomater. Sci.* **2019**, *7* (1), 272.
[34] Y. H. Yang, T. P. Xu, H. P. Bei, Y. J. Zhao, X. Zhao, *Adv. Funct. Mater.* **2021**, *31* (37), 2104636.
[35] a) R. Huang, X. Zhang, W. Li, L. Shang, H. Wang, Y. Zhao, *Adv. Sci.* **2021**, *8* (17), e2100201; b) T. Cui, J. Yu, Q. Li, C. F. Wang, S. Chen, W. Li, G. Wang, *Adv. Mater.* **2020**, *32* (32), e2000982.

Electrosprayed regeneration-enhancer-element microspheres power osteogenesis and angiogenesis coupling

*Tianpeng Xu, Yuhe Yang, Di Suo, Ho Pan Bei, Xiaoxiao Xu, Xin Zhao**

T. Xu., Dr. Y. Yang., D. Suo., H. P. Bei., X. Xu., Dr. X. Zhao.
Department of Biomedical Engineering, The Hong Kong Polytechnic University, Hung Hom, Hong Kong SAR, China
Email: xin.zhao@polyu.edu.hk

We electrosprayed sodium alginate microspheres encapsulating L-arginine doped hydroxyapatite nanoparticles (Arg/HA NPs) and rat bone mesenchymal stem cells (rBMSCs) as regeneration-enhancer-element reservoirs (Arg/HA-SA@BMSC) for bone healing. Such microsphere system can promote the osteogenesis-angiogenesis coupling at the defect site and realize the internal/external modulation loop of encapsulated cells and native cells during bone healing.